Tracking Urban Heat Island Dynamics Using Open Source Tools and Free Data

Sanja Šamanović, Olga Bjelotomić Oršulić, Tera Krajina, Danko Markovinović

Department of Geodesy and geomatics, University North, 42000 Varaždin, Croatia -
(sasamanovic, oborsulic, tkrajina, dmarkovinovic)@unin.hr

Keywords: Urban Heat Islands (UHI), Land Surface Temperature (LST), Normalized Difference Vegetation Index (NDVI), Landsat 8, Free and Open-Source Software (FOSS), Open Earth Observation Data

Abstract

Urban Heat Islands (UHI) represent an increasing challenge in cities worldwide, including smaller urban centres such as Varaždin, Croatia. This study analyses UHI dynamics over a Varaždin city during a ten-year period (2014–2024) using exclusively Free and Open-Source Software (FOSS) and publicly available Earth Observation (EO) data. Landsat 8 thermal imagery was used to calculate Land Surface Temperature (LST), and to analyse its relationship with vegetation cover through the Normalized Difference Vegetation Index (NDVI) and the Proportion of Vegetation (PV). Urban expansion was examined using the Normalized Difference Built-up Index (NDBI). All indices were derived from multispectral and thermal bands using QGIS 3.24 and Python 3.12 libraries including GDAL, rasterio, NumPy, and Matplotlib. The results show a measurable increase in surface temperature, with the average LST rising by +4.41 °C, accompanied by a loss of 3,230 pixels in the dense vegetation class (NDVI > 0.4). Simultaneously, NDBI values indicate expansion of built-up areas across the southern and eastern parts of the city. These changes confirm the spatial transformation towards the urbanization and reduced vegetation cover as main cause of local thermal intensification. This study gives a standardized, open-sourced, transparent and reproducible analysis applicable to other medium-sized cities. The study also explores the potential integration of additional EO sources (Sentinel-3, MODIS, VIIRS) and supporting geospatial data (OpenStreetMap) for enhanced spatiotemporal resolution. The findings highlight the value of FOSS tools and open data in supporting evidence-based urban climate planning and advocate for scalable, cost-effective approaches to UHI mitigation through green infrastructure and adaptive design.

1. Introduction

During the past decades, the rapid expansion of urban development - attributable to population migration - has led to considerable spatial alterations and lifestyle transformations. Such urbanization, where urbanized infrastructure replaces natural cover, brings economic as well as infrastructural advantages but also poses challenges to city management: energy consumption, reduced ecosystem services, pollution, and climate risks.

A key consequence is the Urban Heat Island (UHI) effect, with built-up areas recording higher air and surface temperatures than rural surroundings (Zhou et al., 2017; Oke, 1982). UHI arises from replacing vegetation with impervious surfaces (asphalt, concrete, metal) that absorb and store heat, limiting cooling processes like evapotranspiration and shading. These materials, with low albedo and high thermal mass, retain heat by day and release it at night, intensifying warming. UHI occurs globally, with urban–rural temperature gaps often over 10 °C (Ranagalage et al., 2018; Santamouris, 2020). It alters microclimates, raises cooling energy needs, stresses public health systems, and reduces urban liveability. Hence, integrating microclimatic factors into planning is vital for resilient, sustainable cities (Brigham & Suding, 2023).

Though most evident in large cities, recent studies show smaller ones are also vulnerable—especially where green infrastructure is lacking (Wang, 2019; Kalogeropoulos et al., 2022; Ramos & Cladera, 2022). Key mitigation actions include increasing canopy cover, conserving natural land, and integrating vegetation into urban design. Even minor land-use changes impact local temperatures (Iungman et al., 2023). In Croatia, many medium-sized cities lack formal green infrastructure strategies, missing opportunities to mitigate UHI and protect environmental quality (Gašparović & Jukić, 2022; Kovačić & Štrbac, 2020). Understanding UHI drivers and effects helps local authorities develop targeted adaptations. Effective measures include urban greening, reflective materials, green roofs/facades, water features, and designs promoting air flow and passive cooling. These interventions have reduced heat buildup in both large cities (Shanghai, Warsaw, Vienna) and smaller ones (Bydgoszcz, Reggio Emilia) (Viecco et al., 2021; Zhao et al., 2016; Price et al., 2015; Damyanoic et al., 2016; Mohamed, 2024; European Commission, n.d.).

Croatian studies confirm UHI effects in national urban areas. According to the UHI Mitigation Manual (Ministry of Physical Planning, Construction and State Assets, 2022), key factors include green space loss, heat-retaining materials, climate change, and increasing hot days/nights. A Zagreb case study in Dugave showed microclimatic differences driven by urban form, vegetation, water presence, and building height (UNIC, 2023). Accurate, spatially detailed data are essential for analysing UHI dynamics. Yet, limited budgets often restrict access to high-resolution imagery and proprietary software. Freely available Earth observation (EO) data (e.g., Landsat) and Free and Open-Source Software (FOSS) offer a scalable, transparent, low-cost solution for assessing climate risks. Here, “free” refers not just to cost-free access, but also to the freedom to use, modify, and share data and software, in line with the principles of the FOSS movement. Tools like QGIS allow spatial analysis without expensive licenses, improving accessibility and reproducibility, especially in resource-limited settings. Public EO datasets at various resolutions enable robust assessments, empowering even smaller municipalities to plan adaptations without commercial tools.

This study presents a ten-year spatio-temporal analysis of the UHI effect in the city of Varaždin, in northern part of Croatia, using only free datasets (Landsat 8 from USGS Earth Explorer) and open-source tools (QGIS). It aims to quantify urban–rural surface temperature differences, assess seasonal and interannual UHI variations, and examine vegetation's role in moderating urban heat. Satellite-derived indices like Normalized Difference Vegetation Index (NDVI) and Proportion of Vegetation (PV) Cover are used to evaluate spatial correlations between vegetation and LST.

Analysis uses annual July imagery through the span of ten years period (July 7, 2014, and July 11, 2024), representing peak summer heat and favourable atmospheric conditions for UHI detection (the selected scenes show skies without noticeable cloud cover) (Weng, 2009). The selected years meet three criteria:

- the ten-year interval enables robust trend analysis
- both years experienced exceptionally hot summers, as reported by the Croatian Meteorological and Hydrological Service (DHMZ) (Croatian Meteorological and Hydrological Service).
- 2014 marks the beginning of full Landsat 8 operational coverage with the Operational Land Imager (OLI) and TIRS (Thermal Infrared Sensor) sensors, which are essential for consistent monitoring of surface temperature and vegetation indices (Roy et al., 2014).
-

Also, the city of Varaždin launched initiatives during this period to improve building energy efficiency and promote renewables (Varaždin County Development Agency, 2022).

2. Study area and Data Sources

2.1 Study area

Varaždin lies in northwestern Croatia (Figure 1). The city features a temperate continental climate with warm summers, cold winters, and uniformly distributed yearly precipitation ranging from 900 to 1,000 mm (Climate-Data.org, n.d.). Yearly average temperatures range from 10 to 11 °C. The thermal condition of the city during winter is influenced by recurring fog and high humidity.

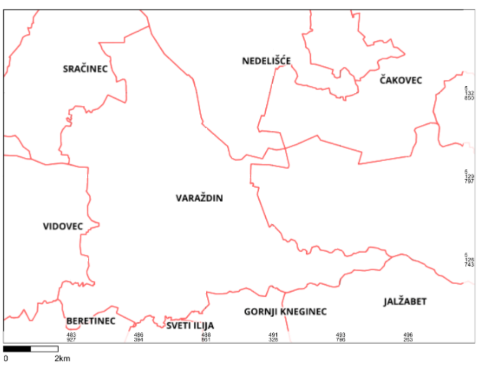

Figure 1. The Area of the City of Varaždin.

Varaždin has a population of around 46,000 (according to the 2021 Census), but like many other middle smaller cities, it's experiencing demographic decline. The city includes a well-preserved historic centre, surrounding residential neighbourhoods, industrial and logistics zones, and green areas on the outskirts. Urban planning faces ongoing challenges, such as scattered spatial development and traffic congestion, while climate change adds further pressure—especially when it comes to managing the UHI effect and stormwater runoff. What makes Varaždin particularly suitable for UHI analysis is its compact form, clearly defined spatial structure, and the availability of freely accessible satellite imagery.

The variation in land cover—from a densely built city centre to vegetated outskirts—enables the comparison of Land Surface Temperature (LST) distribution using tools such as QGIS and Google Earth Engine (GEE) with data from the Landsat mission.

2.2 Data sources

The Landsat 8 satellite is equipped with two main sensors: the OLI and the TIRS. OLI captures information across nine spectral bands (from visible to shortwave infrared), while TIRS records thermal data (Bands 10 and 11), enabling the estimation of LST. The multispectral bands have a spatial resolution of 30 meters, the panchromatic band 15 meters, and each scene spans 185 kilometers in width. The satellite revisits the same location every 16 days, covering the electromagnetic spectrum from visible to thermal infrared: (Visible spectrum - VIS, Near-Infrared spectral band - NIR, Shortwave Infrared spectral band - SWIR, Thermal Infrared - TIR).

Satellite imagery for this study was obtained from the publicly accessible USGS Earth Explorer platform (https://earthexplorer.usgs.gov/). Two sets cloud-free Landsat 8 scenes were selected to represent a decade of change: July 7, 2014 (Path 190 / Row 028) and July 11, 2024 (Path 189 / Row 028) (Table 1). Although the scenes originate from adjacent satellite paths, the overlap at their edges (due to the 185 km scene width) allowed for the selection of spatially corresponding areas. This ensured direct comparability of land surface conditions, despite the slight variation in acquisition geometry.

The use of neighbouring paths was a methodological compromise, driven by the limited availability of cloud-free scenes for the exact same Path/Row and time period. By focusing only on intersecting zones with consistent land cover, the analysis maintains temporal and spatial consistency in evaluating vegetation (via NDVI), urbanization (Normalized Difference Built-up Index, NDBI), and surface temperature (LST). All indices were derived using the same spectral bands: Band 4 (red), Band 5 (near-infrared), Band 6 (shortwave infrared), and Band 10 (thermal infrared).

Scene ID	Date	Band
LC08_L1TP_190028_20140707_20200911_02_T1_B4	2014-07-07	B4
LC08_L1TP_190028_20140707_20200911_02_T1_B5	2014-07-07	B5
LC08_L1TP_190028_20140707_20200911_02_T1_B6	2014-07-07	B6
LC08_L1TP_190028_20140707_20200911_02_T1_B10	2014-07-07	B10
LC08_L1TP_189028_20240711_20240719_02_T1_B4	2024-07-11	B4
LC08_L1TP_189028_20240711_20240719_02_T1_B5	2024-07-11	B5
LC08_L1TP_189028_20240711_20240719_02_T1_B6	2024-07-11	B6
LC08_L1TP_189028_20240711_20240719_02_T1_B10	2024-07-11	B10

Table 1. Selected scenes.

By focusing on intersection areas with consistent land cover, we have ensured a comparability in vegetation characteristics, which is essential for achieving temporal consistency in surface condition analysis.

Visual inspection of the individual spectral bands also provided insight into raw data characteristics and possible seasonal or atmospheric differences. Differences in brightness, contrast, and tone between the two satellite images point to visible changes in land cover, vegetation condition, the extent of urban development, and surface temperature patterns. These variations highlight why spectral analysis is such an important starting point when monitoring UHI effects.

3. Methodology

All data processing and analysis in this study were carried out entirely using FOSS, in accordance with the principles of transparency and reproducibility. The core software used was QGIS 3.34, applied for data visualization, spatiotemporal index calculation, and raster processing. GDAL 3.9 was not used directly, it formed part of the workflow through its integration with QGIS and Python-based tools. It was applied mainly for coordinate reprojection, data format conversion, and working with georeferenced spatial data. For custom operations, the analysis relied on Python 3.12. Several open-source libraries supported this process: rasterio was used to handle raster input and output, while numpy and pandas were responsible for numerical and statistical tasks, respectively. To visualize the results, matplotlib was employed. In the early phase of the study, GEE served as a supplementary platform for preliminary validation, helping to ensure consistency across datasets before the main local analysis was conducted. Although not fully open-source, GEE provides free access to satellite data and supports Python-based workflows, aligning with the principles of the FOSS4G approach.

This study utilizes multispectral data from the Landsat 8 satellite mission, downloaded via the USGS Earth Explorer platform from the Collection 2, Level 1 archive. The analytical framework is based on a multi-step processing workflow that includes the derivation of Top of Atmosphere (TOA) reflectance, Brightness Temperature (BT), PV, and surface emissivity. These parameters serve as input values for calculating three key indices: NDVI, NDBI, and LST, which enable a quantitative assessment of the vegetation, urbanization, and thermal characteristics of the study area.

3.1 Preprocessing of Satellite Data

As a preprocessing step for the analysis, the Digital Number (DN) values of the Landsat satellite imagery were first converted to TOA reflectance. This is done to ensure data comparability over time. The process typically involves a two-step transformation: first, DN values are converted to spectral radiance, and then, if needed, to reflectance using the metadata provided with each scene. For the thermal bands used in LST calculation, only the first step of preprocessing was applied—conversion to radiance—which was subsequently used to derive Brightness Temperature (BT). In contrast, TOA reflectance was calculated from multispectral bands as a standard step for computing NDVI and other indices. Spectral radiance (Lλ) is calculated using the following formula:

$$L\lambda = M_L \cdot Q_{cal} + AL\text{-}O_i \qquad (1)$$

where M_L = multiplicative rescaling factor
Q_{cal} = digital number (DN)
AL = additive rescaling factor
O_i = correction constant

Brightness Temperature is used as an intermediate variable in the calculation of LST. BT is derived from the spectral radiance obtained from the thermal band (Band 10 for Landsat 8), converting radiative energy into temperature expressed in Kelvin:

$$BT = \frac{K_2}{\ln[\left(\frac{K_1}{L\lambda}\right)+1]} - 273.15 \qquad (2)$$

where BT = brightness temperature in °C
K1, K2 = calibration constants (Landsat thermal band)
Lλ = spectral radiance from the thermal band
273.15 = correction factor - Kelvin to degrees Celsius

The resulting BT values represent the temperature as detected from space and include atmospheric effects.

3.2 Calculation of Indices and Surface Parameters

The Normalized Difference Vegetation Index is one of the most popular satellite indices for assessing vegetation activity and land cover condition. NDVI was calculated from Landsat 8 satellite data using the difference in reflectance between band 4 (red, RED) and band 5 (near-infrared, NIR) according to the standard formula:

$$NDVI = \frac{NIR-RED}{NIR+RED} \qquad (3)$$

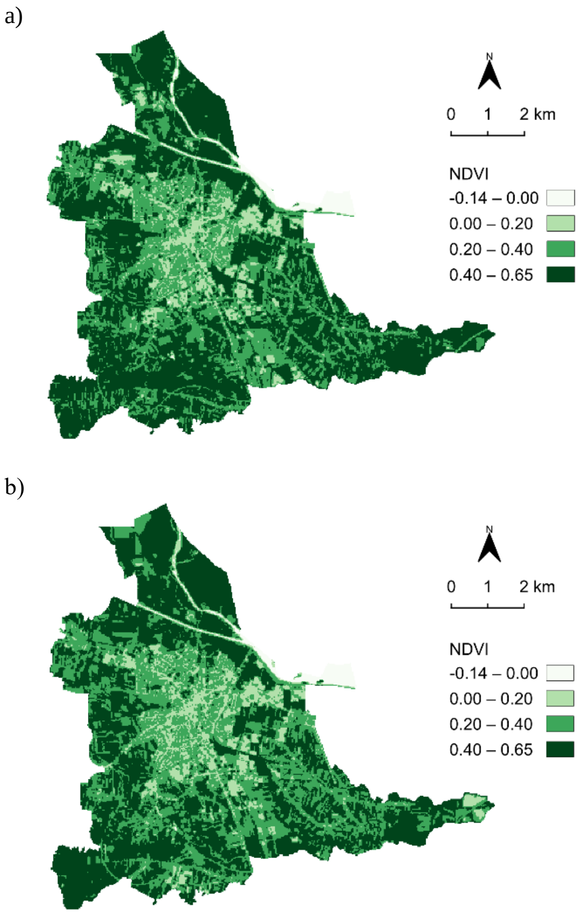

Figure 2. NDVI values on a study area for 2014 (a) and 2024 (b).

Figure 2 shows a comparative display of NDVI values for 2014 (a) and 2024 (b) in the study area. The NDVI maps are visualized using a green color gradient, with darker tones representing denser vegetation and lighter ones indicating sparse or no vegetation.

Healthy vegetation tends to reflect a large amount of NIR radiation while absorbing most of the red light, which creates a clear spectral contrast. NDVI values can range from –1 to +1. Values closer to +1, usually signal areas with dense and healthy vegetation. Values near zero tend to indicate limited or sparse plant cover, while negative values are often linked to non-vegetated surfaces, such as water, exposed soil, or built-up land.

NDVI provides a reliable insight into the spatial distribution of vegetation and, in this study, served as the basis for calculating vegetation cover (PV) and surface emissivity, both necessary for further LST estimation.

The PV is a quantitative measure of vegetation cover fraction within one pixel, calculated from NDVI values. PV is calculated using the formula:

$$P_v = \left(\frac{NDVI - NDVI_{min}}{NDVI_{max} - NDVI_{min}}\right)^2 \quad (4)$$

where $NDVI_{min}$, $NDVI_{max}$ = minimum and maximum NDVI values within the analysed area

The resulting PV has values ranging between 0 (no vegetation cover) and 1 (complete vegetation cover). PV played a dual function: it was used both as an independent indicator of vegetation condition and as an input parameter for calculating surface emissivity, which is required for correcting brightness temperature in the calculation of LST.

Surface emissivity (ε) is defined as the ratio of the actual surface thermal emission to that of an ideal blackbody and is essential for accurately estimating LST. Since various land cover types (vegetation, water, built-up areas) possess different emissive characteristics, pixel-by-pixel emissivity estimation is necessary. Emissivity was determined based on the vegetation proportion index, which estimates the vegetation fraction and its corresponding emissivity. This method assumes a linear relationship between vegetation cover and surface emissivity and is expressed by the formula:

$$\varepsilon = 0.0004 \cdot P_v + 0.986 \quad (5)$$

The resulting emissivity values are applied to correct BT, enabling a reliable estimation of the actual LST. LST represents the estimated physical temperature of the Earth's surface, derived from satellite thermal data. Unlike BT, which includes the influence of the atmosphere and surface emissivity, LST reflects the true thermal characteristics of the surface, corrected for these effects. LST was calculated using thermal band 10 of the Landsat 8 satellite, with emissivity correction (ε):

$$LST = \frac{BT}{1 + \left(\frac{\lambda \cdot BT}{\sigma}\right) \cdot \ln(\varepsilon)} \quad (6)$$

where λ = wavelength of the thermal band used (for Landsat 8: ≈ 10.895×10^{-6} m)
σ = radiation constant 1.438×10^{-2}

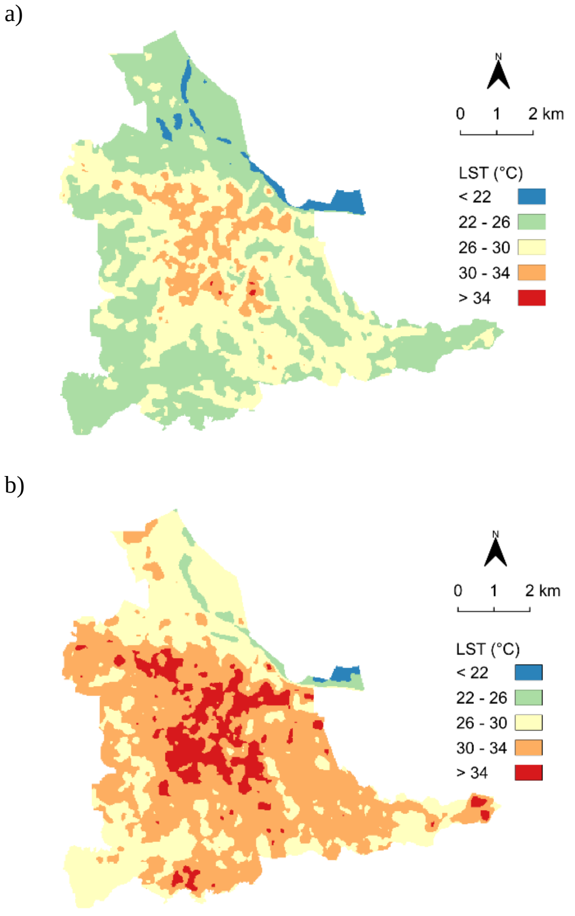

Figure 3. LST for 2014 (left) and 2024 (right).

The results of LST estimation, obtained after applying all the above corrections, are presented in Figure 3, showing the spatial distribution of LST for 2014 (a) and 2024 (b). The maps illustrate a clear temporal increase in LST, especially in urban and low-vegetation areas, highlighting the relevance of emissivity correction and vegetation proportion in thermal analysis.

The NDBI is used to identify and analyse urbanized areas such as buildings, roads, and other artificial infrastructure. The index is based on the reflective properties of materials, where urban surfaces reflect more strongly in the SWIR spectrum, while vegetation reflects more strongly in the NIR. NDBI was calculated using Landsat 8 bands (band 6 – SWIR and band 5 – NIR) according to the formula:

$$NDBI = \frac{SWIR - NIR}{SWIR + NIR} \quad (7)$$

NDBI values range between –1 and +1. Positive values indicate urbanized surfaces (higher SWIR reflectance), while negative values correspond to vegetation or water bodies (higher NIR reflectance). NDBI is not an absolute measure, but a relative index that depends on the context of the area, spatial resolution, time of acquisition, and the sensor used. NDBI was used for detecting built-up areas and for spatial comparison with NDVI and LST layers, aiming to explore the correlation between the degree of urbanization and the increase in LST. Such analysis enables the identification of areas susceptible to the development UHI and provides insights into spatial patterns of urban expansion.

https://doi.org/10.5194/isprs-archives-XLVIII-4-W13-2025-217-2025

a)

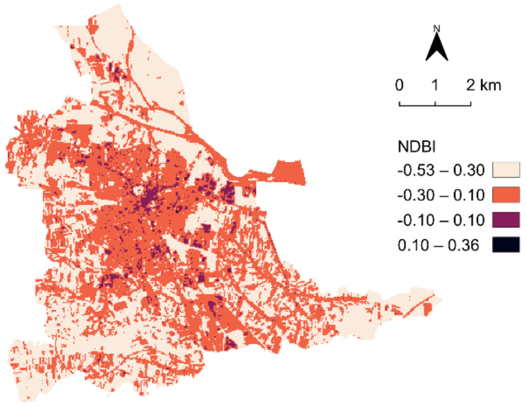

b)

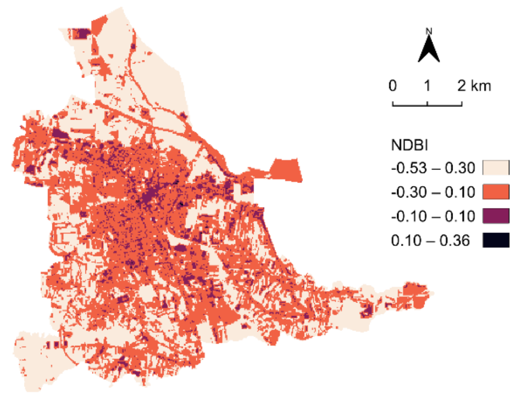

Figure 4. NDBI for 2014 (a) and 2024 (b)

Figure 4 presents the spatial distribution of NDBI values for 2014 (a) and 2024 (b), clearly indicating the intensification and spatial spread of urbanized surfaces over the ten-year period. The comparative analysis of these maps with NDVI and LST results enables a deeper understanding of how urban growth patterns contribute to thermal characteristics and vegetation loss within the study area.

4. Discussion

The analysis of spatial and statistical changes in NDVI, LST, and NDBI indices between 2014 and 2024 reveals transformations in vegetation distribution, urbanization levels, and LST in the Varaždin area. These changes were quantified and visualized through statistical indicators, thematic maps, and classification outputs.

As Table 2 shows, the NDVI decreased slightly from 0.39 to 0.37 (change: −0.014), along with a small drop in range and standard deviation (from 0.136 to 0.135). This indicates a modest decline in vegetation cover, primarily due to a reduction in densely vegetated areas. In addition, the mean LST has increased significantly over the ten-year period. The mean value rose by 4.41 °C, from 26.31 °C in 2014 to 30.72 °C in 2024, accompanied by increases in both minimum and maximum values, from 17.35 °C to 21.23 °C and from 35.53 °C to 39.70 °C, respectively. The increase in standard deviation (from 2.369 to 2.596) reflects growing thermal variability across the area. These results indicate increasing thermal inequality and overall surface warming, with spatial manifestations particularly evident in urban cores and fringe zones.

The mean value of the NDBI increased slightly from −0.19 in 2014 to −0.17 in 2024, while the minimum and maximum values shifted from −0.53 and 0.31 to −0.45 and 0.36, respectively. Standard deviation rose marginally (from 0.106 to 0.119), suggesting a broader spread of NDBI values. These statistical changes align with the observed expansion of built-up areas.

	Year	Min	Max	Mean	SD	Change
NDVI	2014	-0.14	0.65	0.39	0.136	-0.014
	2024	-0.13	0.63	0.37	0.135	
LST	2014	17.35	35.53	26.31	2.369	+4.410
	2024	21.23	39.70	30.72	2.596	
NDBI	2014	-0.53	0.31	-0.19	0.106	+0.017
	2024	-0.45	0.36	-0.17	0.119	

Table 2. Statistical indicators for NDVI, LST(°C) and NDBI

NDVI values were classified according to the standard range (Weier and Herring, 2000) and further adjusted based on the actual value distribution in the dataset. Class descriptions were designed to reflect vegetation characteristics in the specific spatial context. Table 2 shows the analysis of classified NDVI values (Figure 2) confirms the observed trend of vegetation cover change between 2014 and 2024. The number of pixels in the class 4 (dense vegetation class/forests, intensive agriculture) decreased by 3230 pixels (from 36274 to 33044). At the same time, class 3 (medium vegetation cover/grasslands, croplands) and areas in class 2 (low vegetation cove/degraded areas) increased by 2493 and 811 pixels, respectively. The class 1 (no vegetation/built-up or water surface) recorded a minor decrease of 74 pixels. Spatial analysis (Figure 5) further confirms that vegetation loss primarily occurs along infrastructure corridors and urban edges, where built-up areas have expanded at the expense of vegetated cover.

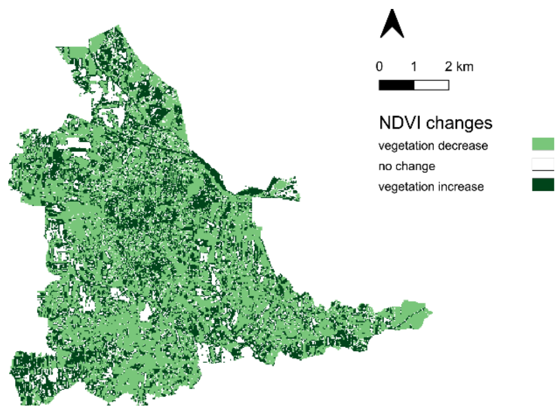

Figure 5. Spatial distribution of NDVI change, 2014–2024.

NDVI class	Values	No. pixel 2014	No. pixel 2024	Change
1	-0.14 – 0.00	1108	1034	-74
2	0.00 – 0.20	5615	6426	+811
3	0.20 – 0.40	23502	25995	+2493
4	0.40 – 0.65	36274	33044	-3230

Table 3. NDVI Classification.

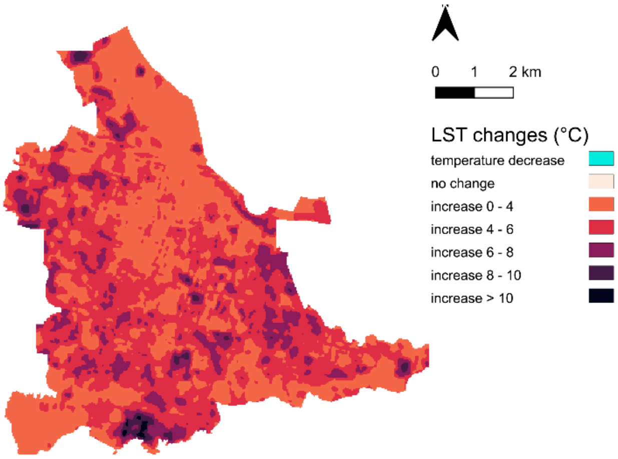

Figure 6. Spatial distribution of LST change, 2014–2024.

The classification of LST values (Table 4) points to a substantial redistribution of surface areas toward higher temperature classes. The number of pixels in class 2 decreased drastically by 31093 (from 32523 to 1430), while class 1 recorded a decline of 1281 pixels. Conversely, the higher temperature classes – class 4 and class 5 – saw a sharp increase of 28852 and 6920 pixels, respectively. The most prominent increases in LST are spatially concentrated in the central and southern parts of the city, as well as along urban fringe zones (Figure 6).

LST class	Values (°C)	No. pixel 2014	No. pixel 2024	Change
1	< 22	1602	321	-1281
2	22 – 26	32523	1430	-31093
3	26 – 30	26576	23178	-3398
4	30 – 34	5748	34600	+28852
5	> 34	50	6970	+6920

Table 4. LST Classification.

The classification of NDBI values was carried out into four classes based on the range of values present in the analysed scenes (2014 and 2024), as well as their spatial distribution and interpretation in relation to visible changes in built-up areas. Although not based on universal thresholds, this approach is commonly applied in the literature when the aim is local-scale spatial analysis of urban sprawl (Zha et al., 2003).

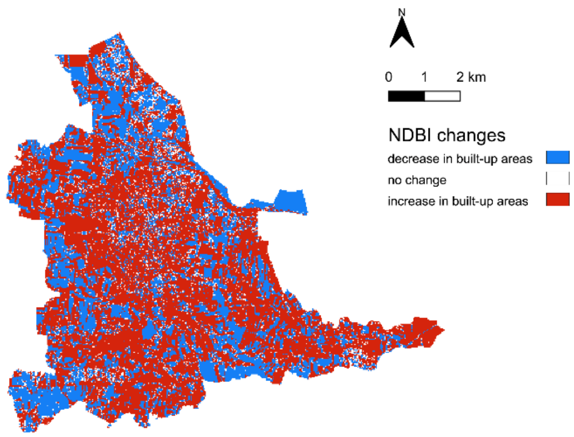

Figure 7. Spatial distribution of NDBI change, 2014–2024.

The spatial map of NDBI changes (Figure 7) clearly visualizes these processes. Red areas, indicating an increase in built-up land, spread across nearly the entire analysed area, particularly in peri-urban zones where residential, transport, and commercial expansion has occurred.

According to the data presented in Table 5, which shows classified NDBI values, the number of pixels in the class 1 (natural or vegetated areas) decreased from 32554 to 28587, representing a loss of 3967 pixels. At the same time, the class 2 (sparsely built-up or transitional zones) increased by 1522 pixels, while the class 3 (moderately built-up urban zones) almost doubled, by 2433 pixels. The class 4 (densely built-up urban cores), although small in absolute numbers, also recorded an increase, from 9 to 21 pixels.

The comparison of thematic NDBI maps for 2014 and 2024 (Figure 4) further confirms these trends. The 2024 map shows a wider spatial extent of higher NDBI values, especially in central parts of the city and along major transport routes. The more evenly distributed light red and red areas in 2024 indicate an expansion of built-up surfaces at the expense of natural and vegetated zones, as also evidenced by the reduction in the number of pixels in the class of natural or vegetated surfaces.

NDBI class	Values	No. pixel 2014	No. pixel 2024	Change
1	-0.53 – 0.30	32554	28587	-3967
2	-0.30 – 0.10	31479	33001	+1522
3	-0.10 – 0.10	2457	4890	+2433
4	0.10 – 0.36	9	21	+12

Table 5. NDBI Classification.

5. Conclusion

Over the past ten years, Varaždin has experienced clear signs of UHI intensification, from higher surface temperatures to shrinking green areas and expanding built-up zones. Between 2014 and 2024, average LST rose by 4.41 °C, while the area of dense vegetation (NDVI > 0.4) dropped by 3230 pixels (approximately 2.91 km²), especially in the southern and eastern parts of the city.

These changes are not evenly distributed. Instead, they reflect fragmented urban growth and increasing thermal pressure in residential and industrial zones. As green areas disappear and construction spreads, heat stress becomes more pronounced – highlighting a direct relationship between land use change and surface temperature rise.

Such disparities point to a growing pattern of thermal inequality, where certain areas (particularly residential and industrial zones) experience disproportionately higher surface temperatures. This trend may be linked to land use intensity, vegetation loss, and infrastructure density, underscoring the need to view heat exposure not only as an environmental issue, but also as a matter of urban equity and public health.

This highlights the urgent need for urban planning to prioritize green infrastructure as an essential part of development, not just an optional addition for the landscaping. The results of this study can support the City of Varaždin in developing urban planning strategies aimed at mitigating UHI effects, such as identifying priority areas for green infrastructure, optimizing land use, and integrating thermal indicators into spatial plans.

By using freely available satellite data and FOSS tools, this study demonstrates that reliable and reproducible analysis is achievable even in with limited access to commercial software, funding, or infrastructure. Future research over the studied area should build on this approach by integrating multi-sensor data, increasing temporal resolution, and developing automated classification and detection models. Such a data-driven and scalable system would enable continuous monitoring of UHI phenomena and more effective urban climate management, ultimately increasing the resilience of medium-sized cities to the impacts of global warming and spatial transformation.

While the use of Landsat 8 imagery and FOSS tools proved effective, the study was constrained by the spatial resolution of 30 meters and the availability of only two summer scenes. Future research should consider multi-temporal approaches and incorporate complementary data sources such as Sentinel-3 or MODIS, which offer improved temporal frequency and day–night thermal information, albeit at coarser resolution.

These satellite missions, while limited in spatial resolution (750–1,000 m), can nonetheless enrich intra-urban UHI research by capturing temporal variability and day–night thermal differences. Open vector datasets such as OpenStreetMap (OSM) offer practical advantages for validating built-up area classifications, particularly at urban edges where satellite data alone may be insufficient. Although these sources were not utilized in this study, their future integration could improve classification accuracy and enable more robust multi-sensor fusion strategies for analysing fine-scale spatial heterogeneity in UHI effects.

Acknowledgements

This research was conducted as part of the scientific project "Potential of Sentinel-1 InSAR Data for Generating Digital Elevation Models in Geodetic Applications", project number UNIN-TEH-25-1-10, funded by the University of North, Varaždin, Croatia.

References

Brigham, J., Suding, K. N., 2023. Cross-scale facilitation: A framework for microclimate moderation of climate change. *Oikos*, 132(5). doi.org/10.1111/oik.10241.

Climate-Data.org, n.d. Climate: Varaždin. https://en.climate-data.org/europe/croatia/varazdin/varazdin-4079/.

Croatian Meteorological and Hydrological Service, n.d. Klima Hrvatske. https://meteo.hr/klima.php?section=klima_hrvatska.

Damyanovic, D., Reinwald, F., Brandenburg, C., Allex, B., et al., 2016. Pilot action city of Vienna – UHI-STRAT Vienna. In: Musco, F. (Ed.), Counteracting Urban Heat Island Effects in a Global Climate Change Scenario, Springer, Cham, 257–280. doi.org/10.1007/978-3-319-10425-6_9.

European Commission, n.d. Reggio Emilia's Climate-Friendly Parks. Covenant of Mayors for Climate and Energy. https://eu-mayors.ec.europa.eu/en/Reggio-Emilia-Climate-Friendly-Parks.

Gašparović, M., Jukić, T., 2022. Uloga zelene infrastrukture u urbanoj obnovi Gornjega grada i Kaptola. *Glasilo Future*, 5(4), 1–10. doi.org/10.32779/gf.5.4.2.

Iungman, T., Cirach, M., Marando, F., Barboza, E. P., Khomenko, S., Masselot, P., et al., 2023. Cooling cities through urban green infrastructure: A health impact assessment of European cities. *The Lancet*, 401(10376), 577–589. doi.org/10.1016/s0140-6736(22)02585-5.

Kalogeropoulos, K., et al., 2022. Urban Heat Island and Thermal Comfort Assessment in a Medium-Sized Mediterranean City. *Atmosphere*, 13(7), 1102. doi.org/10.3390/atmos13071102.

Kovačić, J., Štrbac, A., 2020. Strateški ciljevi gospodarenja urbanim šumama grada Zagreba. *Nova mehanizacija šumarstva*, 30(5), 1–12. doi.org/10.5552/nms.2020.5.

Ministry of Physical Planning, Construction and State Assets, 2022. Priručnik o ublažavanju urbanih toplinskih otoka. https://mpgi.gov.hr/UserDocsImages/dokumenti/NPOO/ZIKGP_NPOO/Prirucnik_UHI.pdf.

Mohamed, M. K., 2024. Urbanization and heat island effect: a comparative study in Egypt. *Int. J. Climatic Stud*., 3(1), 12–23. doi.org/10.47604/ijcs.2479.

Oke, T. R., 1982. The energetic basis of the urban heat island. *Q. J. R. Meteorol. Soc*., 108(455), 1–24. doi.org/10.1002/qj.49710845502.

Price, A., Jones, E. C., Jefferson, F., 2015. Vertical greenery systems as a strategy in urban heat island mitigation. *Water Air Soil Pollut.*, 226(8). doi.org/10.1007/s11270-015-2464-9.

Ramos, B. A., Cladera, L., 2022. Effects of Urban Greenery on Health: A Study from Remote Sensing. *ISPRS Arch. Photogramm. Remote Sens. Spatial Inf. Sci*., XLIII-B3-2022, 17–24. doi.org/10.5194/isprs-archives-xliii-b3-2022-17-2022.

Ranagalage, M., Dissanayake, D., Murayama, Y., Zhang, X., Estoque, R. C., Perera, E., Morimoto, T., 2018. Quantifying Surface Urban Heat Island Formation in the World Heritage Tropical Mountain City of Sri Lanka. *ISPRS Int. J. Geo-Inf*., 7(9), 341. doi.org/10.3390/ijgi7090341.

Roy, D. P., Wulder, M. A., Loveland, T. R., Woodcock, C. E., Allen, R. G., Anderson, M. C., et al., 2014. Landsat-8: Science and product vision for terrestrial global change research. *Remote Sens. Environ.*, 145, 154–172. doi.org/10.1016/j.rse.2014.02.001.

Santamouris, M., 2020. Recent progress on urban overheating and heat island research. *Energy Build*., 207, 109482. doi.org/10.1016/j.enbuild.2019.109482.

UNIC, 2023. Urban Heat Islands in Dugave, Zagreb. https://www.unic.eu/storage/app/media/GREEN%20ZAGREB_ECOLOGICAL%20RISKS/Urban%20heat%20islands%20workshop.pdf.

Varaždin County Development Agency, 2022. Spatial Plan of Varaždin County. https://zzpuvz.hr/wp-content/uploads/2022/01/1-ppz-varazdinske-zupanije-osnovni.pdf.

Viecco, M., Jorquera, H., Sharma, A., Bustamante, W., 2021. Green roofs and green walls layouts for improved urban air quality by mitigating particulate matter. *Build. Environ*., 204, 108120. doi.org/10.1016/j.buildenv.2021.108120.

Wang, Z. F., 2019. The relationship between land use, land cover change, and the heat island effect in Xi'an City, China. Appl.

Ecol. Environ. Res., 17(4), 7795–7806. doi.org/10.15666/aeer/1704_77957806.

Weier, J., Herring, D., 2000. Measuring Vegetation (NDVI & EVI). NASA Earth Observatory. https://earthobservatory.nasa.gov/features/MeasuringVegetation

Weng, Q., 2009. Thermal infrared remote sensing for urban climate and environmental studies: Methods, applications, and trends. *ISPRS J. Photogramm. Remote Sens*., 64(4), 335–344. doi.org/10.1016/j.isprsjprs.2009.03.007.

Zha, Y., Gao, J., Ni, S., 2003. Use of normalized difference built-up index in automatically mapping urban areas from TM imagery. *Int. J. Remote Sens*., 24(3), 583–594. doi.org/10.1080/01431160304987.

Zhao, M., Cai, H., Qiao, Z., Xu, X., 2016. Influence of urban expansion on the urban heat island effect in Shanghai. Int. *J. Geogr. Inf. Sci*., 30(12), 1–21. doi.org/10.1080/13658816.2016.1178389.

Zhou, B., Rybski, D., Kropp, J. P., 2017. The role of city size and urban form in the surface urban heat island. *Sci. Rep*., 7(1). doi.org/10.1038/s41598-017-04242-2.